

Global metabolic optimality in the structure of the coronary arteries

Jonathan Keelan,¹ Emma M. L. Chung,² and James P. Hague¹

¹*Department of Physical Science, The Open University, Milton Keynes, UK, MK7 6AA*

²*Department of Cardiovascular Sciences,
University of Leicester, UK, LE1 5WW*

The structure of the large coronary arteries is both heritable and reasonably consistent between individuals, but the extent to which this results from evolutionary pressure towards an energy-efficient, globally-optimal, structure is unknown. We present an algorithm for the determination of an energetically globally optimal arterial tree in arbitrary tissue geometries. We demonstrate through application of the algorithm that it is possible to generate *in-silico* vasculatures that closely match porcine anatomical data on all length scales. We therefore conclude that evolutionary pressure has resulted in a near globally optimal structure of the larger coronary arteries. We also examine the effect of changing length scales, predicting that the structures of the coronary arteries can change from a meandering form for small animals to very straight vessels for large animals. The method presented here is not limited to hearts, and represents a major advance in modeling the arterial vasculature, that could have important applications for medical imaging analysis and the design of artificial organs.

Arterial trees are vital for the transport of oxygen and nutrients to tissue. Their anatomy has been studied for many centuries through the dissection of cadavers, inspection of corrosion casts, medical imaging techniques, and computational models. The structure of the large coronary arteries has been found to be heritable [1] and it is known that individual arterial bifurcations follow optimality principles that lower metabolic demand locally [2–8], as demonstrated by the scaling laws followed by arterial trees [9–13].

More recently, there has been increased interest in mimicking arterial growth (angiogenesis) to simulate microvasculature anatomy and aid interpretation of medical images [19]. These models are created based on local optimization principles, where the anatomy of each branch in the arterial tree is governed by a compromise between maximizing fluid dynamical efficiency and minimizing the quantity of blood required. It can be shown that local minimization of the power required to pump blood through arteries plays a key role in governing the properties of individual bifurcations. However, models of coronary vasculature, based on local optimization are not able to explain if the organization of major arteries is the result of fluid dynamical optimization across the ‘whole organ’ [14–18].

The relationship between the radii of vessels in individual bifurcations is well described by Murray’s law: $r_p^\gamma = r_{d_1}^\gamma + r_{d_2}^\gamma$ where r_p is the radius of the parent artery, $r_{d_{1,2}}$ those of the daughter arteries and γ is the bifurcation exponent [4, 20]. Current standard methods for ‘growing’ computer generated vascular trees into a simulated tissue substrate aim to optimize the local properties of individual bifurcations [17, 21], but create arterial branches that are more symmetrical than those found in nature [22] and significant extensions are required to generate vessels in hollow organs [23]. To ameliorate these problems, local optimization schemes have been extended to incorporate minimization of global energy expenditure through occasional ad-hoc reshuffling of arterial bifurcations. These schemes generate arterial trees that are marginally more realistic in appearance, but do not recreate large scale features in organ-specific vasculature. These algorithms also invoke numerous constraints and provide no guarantee of arriving at a final structure that is globally optimized to supply the entire organ [24]. Development of a model which reaches a morphologically accurate solution based solely upon optimization criteria would represent a major breakthrough in vascular research, facilitating modeling of realistic vascular trees in organs lacking extensive morphological databases, and enabling accurate computer-assisted segmentation of arteries from medical imaging data. This could provide valuable insights into currently unanswered

questions regarding angiogenesis, vascular structure, and physiology. This paper introduces a novel method for generation of ‘whole organ’ arterial trees, in any arbitrarily shaped tissue substrate, that obey both local and global optimization criteria. As an example application we determine the theoretically optimal configuration of arteries for supplying the heart and compare our computer generated coronary vasculature with morphological data from real coronary arteries. Specifically, we investigate whether the observed anatomy of the coronary arteries is similar to that expected from global minimization of total energy expenditure. This addresses a key question in evolutionary biology, which supports the view that genetic coding for the circulatory system emerges purely as a result of evolutionary pressure towards optimal cardiovascular efficiency.

The main goal of any arterial tree is to maintain adequate perfusion of blood while minimizing total metabolic expense. The suitability of a given arterial tree for this purpose is governed by the following considerations: (1) Since blood is viscous, the power required to pump blood through the vasculature should be minimized, (2) as energy is required for the generation and maintenance of blood, the volume of blood required should be minimized. Therefore, a successful algorithm seeks to minimize both the power required to pump blood through the whole tree and blood volume, so that trees with a lower total metabolic demand are chosen more favorably. Murray’s law achieves this for individual bifurcations, but the optimal organization of large numbers of connected bifurcations is far from obvious. The interplay between these competing concerns for thousands of arterial segments leads to a complex optimization problem.

To identify globally optimized arterial trees, we use a powerful computational technique borrowed from condensed matter physics, known as Simulated Annealing (SA) [25]. Although SA is computationally expensive, correctly applied SA techniques have a key advantage of being mathematically proven to converge to a global energy minimum. To achieve this, our SA algorithm searches all possible topologies and geometries for arterial trees, ranging from perfectly symmetric, intricately bifurcating structures, to asymmetric trees characterized by a single trunk vessel (i.e. the algorithm is ergodic). This is achieved by allowing: (1) repositioning of bifurcations, and (2) swapping the parent vessels of bifurcations between different parts of the tree. By introducing these forms of plasticity to our models, the entire parameter space of the tree can be explored, allowing the algorithm to identify the best possible arterial configuration for supplying a particular organ. Full details of this

novel method can be found at the end of the article.

An advantage of using SA compared to previous techniques is that very few parameters and constraints need to be defined before initiating the SA search. For modeling the coronary arteries these included: (1) A tissue substrate representing an ellipsoidal human heart muscle of mass 218g, constructed based on physiological parameters [26] . The right ventricle was assumed to take the form of a super ellipsoid of exponent 2.5 and the left ventricle was represented by a simple ellipsoid. Truncation of the ellipsoidal model was chosen so that the mass of the tissue corresponded to a reasonable physiological value given morphological data for ventricle thickness. (2) Blood flow through each of the terminal segments of the tree was assumed to be constant, with each arteriole supplying an equal volume of tissue and homogeneous perfusion throughout the tissue parenchyma [27]. These assumptions greatly simplify fluid dynamical calculations for estimating the total power needed to pump blood through the tree. (3) The metabolic cost of maintaining a given volume of blood was assumed to be $641.3 J s^{-1}$ per metre cubed of blood [28] . For convenience, each arteriole supplies a sphere of tissue with a size calculated by assuming a mean blood flow per unit volume for cardiac muscle of $0.8 ml min^{-1} g^{-1}$ [29]. (4) The larger arteries with diameters greater than 0.01mm were constrained to avoid penetration of the outer layer of heart tissue. This simplification differs slightly from real coronary vasculature, where progressive intrusion of arteries into the myocardium can be observed [30]. However, as the major arteries modeled by our algorithm are far larger than the intra-myocardial vessels, a sharp cut-off is thought to provide a reasonable approximation. (5) The starting positions of the two root arteries were fixed with a total input flow of $4.16 \times 10^{-6} m^3 s^{-1}$ [31]. Relative radii of the two inputs to the tree were constrained via $r_1^2 + r_2^2 = [2.1mm]^2$ however, the relative sizes of root arteries and division of perfusion territories are determined by the algorithm alone. (6) The branching exponent varies throughout the coronary arterial tree, but for the larger arteries its value remains in the range 1.8 to 2.3. A variable branching exponent would greatly increase the computational cost of the algorithm, so a medial value of 2.0 was chosen for the entire tree [11].

Coronary arterial trees containing increasing total numbers of vessels grown using the SA algorithm are presented in Fig. 1. In real human coronary trees, there are 3 identifiable main coronary arteries (see e.g. the schematic from Ref. [32]): Left Anterior Descending (LAD), Right Cardiac Artery (RCA) and Left Circumex Artery (LCX). The positions and

relative dimensions of these are similar in most humans, with major variations observed in less than 1% of healthy individuals [33]. Trees grown using SA (Fig. 1) adhere well to this structure. There is a consistency in the placement of the larger arteries, although the RCA appears slightly lower and the right marginal artery appears slightly shorter in our models. Overall, visual inspection of the arterial structure appears extremely promising.

To provide a quantitative comparison of our trees with anatomical data, the topological characteristics of the computer generated coronary artery trees were extracted and compared to morphological data characterizing the pig coronary arteries published by Kassab et al. [11]. Porcine cardiac morphology is thought to be very similar to that of humans. Kassab and colleagues used a combination of corrosion casting and optical sectioning to obtain detailed morphometric data, tabulated using the Strahler (or stream) ordering scheme to denote elements of the tree of varying scale. Within this scheme, the lowest Strahler order numbers correspond to the smallest arterioles and the largest numbers refer to major vessels. To directly compare arterial diameters, lengths and branching properties of our computer-generated arterial tree with real data from pig coronary arteries, averages were obtained over all elements of the same Strahler order.

The mean vessel diameters as a function of order number, averaged over multiple trees comprising 6000 arterioles (12000 vessel segments) are shown in Fig. 2(a). Excellent agreement is found between the trees generated in-silico and the morphological data. Only slight deviations from the morphological data can be seen for the smallest vessels (lowest order arteries) in the generated tree. This is likely to be due to the combination of integer order numbers and the condition that terminal sites are of constant radius. The result of this constraint is that the terminal radii will only match the anatomical data for a correct choice of the number of arterioles. Fig 2(c) shows the effects on diameter of increasing the number of arterioles from 500 to 2000. Agreement is generally good, regardless of the number of terminal arteries, and there is a clear trend towards matching the experimental data as simulated tree size increases. Fig 2(b) compares average vessel length in the model and porcine morphological data as a function of order number. For the largest arteries (high order numbers) the agreement is excellent. Although the lengths of the smaller arteries (Strahler orders < 7) in the computer generated tree tended to be overestimated, this can be easily explained by the fact that the smallest vessels are required to bridge a gap that would normally be filled by inclusion of lower order vessels in a larger simulation. As the

number of generated vessels is increased, the agreement with morphological data improves (Fig. 2(d)).

Previously, the best methods available for the computer generation of arterial trees struggled to recreate realistic branching asymmetry. Fig 3 shows the ratio of daughter to mother vessel radii for the largest and smallest daughter vessels as a function of order number. This provides a measure of the branching asymmetry of the tree, where small ratios indicate that branching is symmetric, while ratios approaching 1 suggest a large trunk vessel with small branches. For Strahler orders corresponding to microvascular arterioles, both the computer generated and true morphology approach 0.7, which is consistent with perfectly symmetric branching where both daughter vessels are of similar size. Agreement with the morphological data from Ref. [34] improves as the size of the computer generated tree increases. This is not the result of any special input parameters or initial conditions. The trees are topologically and spatially randomized before SA optimization begins, and are allowed to explore the entire parameter space during optimization. The observed asymmetry is purely the result of a balance between pumping power and metabolic maintenance cost, and is a major improvement in predicting the trunk-like structure of major vessels.

Our final figures show the effect of altering the metabolic energy cost of blood per unit volume m_b . The change in m_b can also be interpreted as a change in length scale (see method section), e.g. a mouse sized heart vs a pig heart. The largest morphological change is found in the lengths of the larger arteries (Fig 5). As m_b increases, bifurcation symmetry is also increased in the larger arteries and as a result there is an increase in the number of Strahler orders present in the tree (Fig 5). The explanation for these scaling behaviours is evident when considering the limiting cases. For $m_b = 0$ the power involved in pumping the blood dominates the optimisation, which leads to a large, snaking artery with small side branches that supply the tissue. This large artery would cover the entire surface of the heart, and the configuration is equivalent to a completely asymmetric binary tree. For a large m_b value (or small power cost) there is a huge penalty associated with larger arteries, and so their lengths are contracted. In order to accommodate the reduction in length, the larger arteries must bifurcate more frequently and symmetrically. Additionally the high volume cost causes the trunk artery to minimise its total length, resulting in a much straighter path across the tissue. Less extreme examples of this behaviour can be seen in Fig 4, with meandering arteries for small m_b and straight arteries for large m_b . Since changing m_b is equivalent to

changing the length scale, these results are likely to mean that there are structural differences between species of different sizes, as the power required to pump blood becomes relatively more important than the metabolic demand to maintain blood volume in small vessels. In the absence of morphological data, visual inspection of the coronary arteries in Swiss albino mice tentatively indicates that vessels meander around in such a way in smaller species [35] and in donkeys indicate that vessels are straight in larger species [36].

In summary, we have developed a new algorithm for growing arterial trees *in-silico*, which is capable of identifying the globally optimal configuration of arteries for any arbitrarily shaped organ. The resulting coronary arterial tree is fully optimized with respect to metabolic processes, subject to the condition that all tissue receives sufficient blood flow to fulfill metabolic demands. Agreement between the morphology of coronary arterial trees generated *in-silico* and data from real coronary arteries was excellent and improves as the number of vessels modeled increases. Comparison with real arterial trees supports the view that the overall layout of the coronary arteries results from evolutionary pressure towards an optimal configuration with few vestigial remnants. While the number of major anatomical variations in human coronary arteries is small ($< 1\%$), there is scope for applying our model to assessing the effects of anatomical variations on the risk of coronary artery disease. Further work is also required to generate arterial trees for other organs and to incorporate subject specific tissue geometries. Ultimately, these models may help to improve the interpretation of medical images through advanced image segmentation techniques, to reveal new avenues for the modeling and evaluation of cardiovascular physiology, and could be used to design and print efficient vasculatures for artificial organs.

METHOD

Note that in the following, bifurcations will be referred to as nodes, arteries will be referred to as segments between nodes, and terminal arterioles are referred to as end nodes.

Metabolic cost to maintain blood volume

The first component of the algorithm involves calculating the power needed (metabolic cost) to maintain the entire tree, which will be used as a value in the cost function. The

power consumption of the tree can be split into two separate parts: the first is the metabolic cost of maintaining the volume of blood and tissue associated with the tree, and the second is the power required to pump blood through the tree. In order to calculate the volume, the length and radius of each segment (vessel) i of the tree must be known, however by assuming a fixed bifurcation exponent, the radii are determined by the topology and it is only the lengths which rely on the geometrical arrangement. In order to convert the volume to a cost, it must be multiplied by a physiologically reasonable value m_b corresponding to the metabolic demand of the same quantity of blood and vascular tissue [28]. Thus the metabolic cost due to the volume of the tree will be given by:

$$C_v = m_b V_{tree} \quad (1)$$

where m_b is taken to be $641.3 \text{ J s}^{-1} \text{ m}^{-3}$ and V_{tree} is the volume of the entire tree.

Power cost to pump blood through vessels

To calculate the power needed to pump blood through the entire tree, we must know the pressure and volumetric flows inside each segment (vessel) of the tree, which can be found by first assuming that Poiseuille's law, $\Delta p = QR$, is followed inside the segments, where Δp is the pressure drop over the vessel, and Q is the flow. Due to the application of Murray's law and the assumption that terminal node flows are constant, the procedure for calculating the relevant fluid dynamical quantities is greatly simplified: the only quantity which relies on the geometrical arrangement of the tree is the pressure. In a sense, the segments can be considered as connected set of resistors, with the resistance given by:

$$R = \frac{8\mu L}{\pi r^4}, \quad (2)$$

where r is the radius of the vessel, L its length and $\mu = 3.6 \times 10^{-3} \text{ Pas}$ the viscosity of blood. The pressures for every node in the tree can then be found recursively. Knowing the pressure, resistance and flow of each segment, the power consumed by each segment i can be easily calculated according to:

$$W_i = Q_i^2 R_i, \quad (3)$$

where W_i is the power consumed by segment i . Summing over all segments in the tree, we find the total power required to maintain the proper flow through the tree is given by:

$$C_w = \sum_i^{N_{tot}} W_i. \quad (4)$$

Ensuring tissue supply

The primary purpose of the vascular tree is to supply blood, thus it is important to ensure that terminal nodes are correctly dispersed inside the tissue. Initially, terminal nodes are randomly distributed inside the tissue, with each node having associated with it a sphere of influence for blood supply. The radius of this sphere is calculated using physiological values for the blood demand of the tissue under consideration. The density of myocardium is $\rho = 1.06 \times 10^3 \text{ kg m}^{-3}$ [37], and the flow demand is $1.13 \text{ ml min}^{-1} \text{ g}^{-1}$ [38] leading to a flow demand per m^3 of heart tissue of $q_{\text{required}} = 1.3 \times 10^{-5} \text{ m}^3 \text{ s}^{-1}$. The total flow into the heart is $Q_0 = 4.16 \times 10^{-6} \text{ m}^3 \text{ s}^{-1}$ [39], which can be converted to total flow per node as $Q_N = Q_0/N$, where N is the total number of arterioles (end nodes). The radius of the supply sphere is then calculated via $4\pi R_{\text{supply}}^3/3 = Q_N/q_{\text{required}}$. The sphere can be thought of as a microcirculatory black box [17], where the exact fluid dynamical details of the blood flow have been ignored. Spheres of blood supply associated with end nodes are stored in a voxel map (a voxel is a 3D generalization of a pixel) of the tissue, where each terminal node adds exactly one to each voxel inside its sphere of supply. The terminal nodes are then allowed to move inside the tissue, where after each move a new voxel supply map is calculated, and the overlap (each voxel supplied by more than 1 sphere) is used as a value in the cost function of the simulated annealing algorithm. In addition, all voxels not being supplied are given a cost, so that as a whole the penalty associated with having both unsupplied and oversupplied voxels is given by:

$$C_s = \sum_{\text{voxels}} s; s = \begin{cases} 10 & \text{if } b = 0 \\ (b - 1)^2 & \text{otherwise} \end{cases} \quad (5)$$

where b is the value of the supply at the voxel and the sum is performed over all the voxels comprising the tissue. C_s is then a value defining the fitness of the tree in terms of its ability to supply blood, and the penalty for oversupplying voxels forms a sort of self avoidance algorithm, where terminal nodes are encouraged to pack the tissue as densely as possible

without overlapping. A benefit of this method is that it allows easy integration of medical imaging into the model, as well as providing an easy method for differentiating tissue with different blood supply demands.

Exclusion of large vessels from tissue

In order to create a realistic vascular tree, it must be possible to exclude some segments from penetrating the tissue. For instance, in the case of the heart, it would be unlikely to find a very large artery within the myocardium, and vessels may not penetrate the ventricles; rather, the larger arteries and arterioles lie on the surface of the heart, with only the smaller arterioles and capillaries being found inside the tissue. To mimic this structure, the algorithm makes use of a cut off radius R_{cutoff} , where it is decided that segments with radius larger than this can not penetrate the tissue. In the work presented here, $R_{\text{cutoff}} = 0.01\text{mm}$. To determine which of the segments with radius greater than R_{cutoff} has penetrated the tissue we first take a distance transform of the tissue surface for each tissue voxel. This provides a second voxel map of the tissue, distinct from the blood supply map, which gives a measure of how far a point is away from the surface when it is inside the tissue (outside of the surface, the value is zero). For each segment satisfying the radius criteria, a list of voxels which its center-line penetrates is generated [40] along with a value for the length element of the segment present inside that voxel. A cost is then calculated based upon the value of the distance transform at each of the voxels according to,

$$C_o = \pi r^2 (D_{i,j,k} W_{i,j,k})^6, \quad (6)$$

where i , j and k are the x , y and z voxel coordinates taken from the centerline of the segment. D_{ijk} is the value of the distance transform at that voxel coordinate. W_{ijk} is the length of the segment spent inside the voxel. The sum is performed over all the voxels contained in the list calculated from the center-line. This cost can then be used in the algorithm as a penalty, which makes moves taking large segments out of the tissue favorable. While this approach does not account for arteries whose diameters intersect multiple voxels, for the voxel resolutions used in the model (1mm) it is entirely appropriate given that the larger diameter vessels are small in number and of a similar size (2mm).

Pressure constraints

In physiologically realistic trees, capillary networks should receive a constant pressure at the inputs to function correctly. In order to ensure that a constant pressure P_{term} is found at the terminal nodes, a new cost can be devised. The quantity must be a positive definite function of the sum of the difference between the ideal end node pressure P_{term} and the actual terminal node pressure of node i : P_i . A suitable candidate is then given by:

$$C_p = \sum_i^{N_{term}} (P_i - P_{term})^2, \quad (7)$$

where the sum is performed over all terminal nodes. In practice, for trees which can be realistically optimized on feasible time scales (i.e of a few thousand nodes), the pressure drop from root to end node is less than 1% of the total pressure drop of a real arterial tree, with the bulk of the pressure drop occurring over smaller arterioles than those considered here. It is then unnecessary to perform this calculation, however when it becomes possible to grow larger trees the pressure at the capillaries to be taken into consideration. This will add a significant computational cost.

Total cost function

We have now determined a form for all the relevant costs associated with an arbitrary tree configuration supplying arbitrary tissue shapes. We can therefore define a total cost which gives a numeric measure of the fitness of a given tree, defined as:

$$C_T = A_{w,v}(C_w + C_v) + A_o C_o + A_p C_p + A_s C_s \quad (8)$$

where A_i indicates a weighting value which scales each relevant cost. There is no way to analytically determine what weights to use, and the selection of appropriate weights must be found experimentally, however a few basic principles such as the having a very high weight for the blood supply cost and a low weight for the end node pressure cost can guide the process. In this work, we use $A_{w,v} = 1$, $A_p = 0$, $A_s = 1 \times 10^{18}$ and $A_o = 1 \times 10^{13}$. In this way, A_s and A_o force the exclusion of vessels and uniform supply of tissue to act like constraints.

Simulated annealing

Consider the values of the cost function laid out for different shapes of the tree (the parameter space) and there will be a landscape of peaks and valleys. A naive approach to finding the solution with the least metabolic cost would be to systematically alter the properties of the tree, and always select trees where there is even the smallest improvement to the fitness (a downhill search). However, this approach typically leads to solutions that fall into local valleys in the parameter space. To select the fittest, globally optimized, trees, we use a powerful technique for optimization problems known as simulated annealing (SA) [41]. The primary difference between SA and a downhill search is that SA also spends some time exploring solutions with higher cost function, and in this way can climb out of shallow valleys in the fitness function to explore other deeper regions, eventually finding the global minimum.

The total cost C_T will play the role of energy in the simulated annealing algorithm, so that the probability of accepting a change to a tree of cost C_T^i , resulting in a tree of cost C_T^f is given as

$$P_i^f = \begin{cases} \exp\left(-\frac{\Delta C_T}{T}\right) & \text{if } \Delta C_T > 0 \\ 1 & \text{otherwise} \end{cases} \quad (9)$$

Where P_i^f is the probability of going from state i to state f , $\Delta C_T = C_T^f - C_T^i$ is the change in the cost function associated with going from state i to f , and T is the simulated annealing temperature parameter. It is this small probability to accept a higher cost tree during update that allows the tree to climb out of local valleys in the cost function. The algorithm then proceeds by making changes to the tree structure, calculating the change in cost function, and then either accepting or rejecting the change by comparing the probability above to a random number between 0 and 1. T starts large and is reduced slowly. If T has been reduced sufficiently slowly, then the global minimum of the cost function will be reached. Here, the highest T is 1×10^{28} , the lowest is 10^{-22} and the maximum number of updates attempted is 10^9 .

Exploring the tree structure: Translations and node swaps

In order for the simulated annealing algorithm to work, it must have access to set of moves which allow it to alter the configuration of the tree. It is necessary to find changes that can be made to the topological and geometrical structure of the tree such that all possible solutions, between perfectly symmetric structures and a single trunk vessel can be explored (i.e. the algorithm is ergodic). This is achieved by allowing: (1) repositioning of bifurcations, and (2) swapping the parent vessels of bifurcations between different parts of the tree. The first of these moves is simple: translate a node in space. For every type of node this move is possible, so that each node is allowed to explore the entire physical space. The second move is performed by swapping the parents of two nodes. For all nodes but the root node, this move is valid, and performed consecutively it allows all possible tree topologies to be explored. If one of the two nodes is a direct parent of the other (i.e while traversing up the tree to the root node from one of the chosen nodes, the other node is encountered), then the move is rejected as the tree resulting from the move would form a closed loop. With these two modifications, the entire parameter space of the tree can be explored, allowing the algorithm to reach a globally optimal solution.

Strahler order

We briefly introduce Strahler (or stream) order here. This ordering method was first introduced to classify river systems, but can be applied to any bifurcating system such as an arterial tree. In a standard Strahler ordering, nodes at the end of a tree (in this case the arterioles) are assigned a number 1. At a bifurcation, if two vessels (segments) of the same order meet, then the order of the parent vessel is 1 higher. However, if two vessels of different orders meet, the artery supplying these vessels has the largest order of the two. For example, if two arteries of order 1 meet, then the vessel supplying these arteries has order 2. If an artery of order 3 meets an artery of order 1, then the vessel supplying these arteries has order 3. An example is shown in the diagram. Therefore, within this scheme, vessels with the lowest order are arterioles. The major vessels have the largest order. The Strahler order used here is then diameter adjusted following the approach in Ref. [42].

Within the Strahler ordering scheme it is possible to identify continuous sections of vessels

which possess the same order number. These are referred to as elements, so that a single arterial element may pass through multiple bifurcations. Throughout this article it is the properties of elements which will be calculated for direct comparison with Ref. [11]. We note that due to the early termination of the simulated trees, calculated order numbers are modified so that the root nodes have an order number equivalent to that of the largest arteries of real coronary arterial trees. For example, in the work of Kassab, the largest diameter defined Strahler order number is 11, corresponding to the input artery. For a computer generated tree of only 6000 nodes spanning order numbers 1-6, 5 must be added to each order number so that the orders of the root nodes (largest vessels) match and a direct comparison can be made. This is consistent with assuming that the smallest vessels in the computer generated tree correspond to order 6 vessels due to smaller vessels downstream of the smallest vessels in the in-silico model.

Equivalence of change in length scale and change in m_b

Once the large vessels have been excluded from the tissue and all tissue is supplied, the remaining cost function that is optimised has the form,

$$C = m_b \pi r^2 l + \frac{8\mu l Q^2}{\pi r^4}$$

now, make the transformations, $r \rightarrow r' = Ar$, $l \rightarrow l' = Al$. Then the cost function becomes,

$$C = A^3 m_b \pi r^2 l + \frac{8\mu A l Q^2}{A^4 \pi r^4}$$

since the optimum in the cost function is the same independent of a multiplicative factor that acts on all terms, then we can absorb a factor of $1/A^3$ into the cost function to obtain:

$$C' = A^6 m_b \pi r^2 l + \frac{8\mu l Q^2}{\pi r^4}$$

identifying a new $m'_b = A^6 m_b$ the cost function now has the same form. This demonstrates that changing the metabolic constant m_b is equivalent to changing the length scale of the problem.

-
- [1] R Glenny, S Bernard, B Neradilek, and N Polissar. Quantifying the genetic influence on mammalian vascular tree structure. *Proceedings of the National Academy of Sciences of the United States of America*, 104(16):6858–6863, 2007.
 - [2] M. Zamir. *The Physics of Pulsatile flow*. Springer, 2000.
 - [3] MDS Frame and IH Sarelius. Energy optimization and bifurcation angles in the microcirculation. *Microvascular research*, 50:301–310, 1995.
 - [4] C D Murray. The Physiological Principle of Minimum Work: I. The Vascular System and the Cost of Blood Volume. *Proceedings of the National Academy of Sciences of the United States of America*, 12(3):207–14, March 1926.
 - [5] N Kizilova. Common Constructal Principles in Design of Transportation Networks in Plants and Animals. (September):1–12, 2008.
 - [6] S Rossitti and J Löfgren. Vascular dimensions of the cerebral arteries follow the principle of minimum work. *Stroke: A Journal of Cerebral Circulation*, 24(3):371–377, 1993.
 - [7] G S Kassab, C A Rider, N J Tang, and Y C Fung. Morphometry of pig coronary arterial trees. *American Journal of Physiology*, 265(1):H350–65, 1993.
 - [8] F Cassot, F Lauwers, S Lorthois, P Puwanarajah, V Cances-Lauwers, and H Duvernoy. Branching patterns for arterioles and venules of the human cerebral cortex. *Brain research*, 1313:62–78, February 2010.
 - [9] Y Huo and G S Kassab. Intraspecific scaling laws of vascular trees. *Biomedical Engineering*, (June 2011):190–200, 2012.
 - [10] Y Huo and G S Kassab. A scaling law of vascular volume. *Biophysical journal*, 96(2):347–53, January 2009.
 - [11] G S Kassab. Scaling laws of vascular trees: of form and function. *American journal of physiology. Heart and circulatory physiology*, 290(2):H894–903, February 2006.
 - [12] H U Bengtsson and P Edén. A simple model for the arterial system. *Journal of theoretical biology*, 221(3):437–43, April 2003.
 - [13] G B West, J H Brown, and B J Enquist. A General Model for the Origin of Allometric Scaling Laws in Biology. *Yeast*, 122(1997), 2011.

- [14] R Karch, F Neumann, M Neumann, and W Schreiner. A three-dimensional model for arterial tree representation, generated by constrained constructive optimization. *Computers in biology and medicine*, 29(1):19–38, January 1999.
- [15] R Karch, F Neumann, M Neumann, and W Schreiner. Staged growth of optimized arterial model trees. *Annals of Biomedical Engineering*, 28(5):495–511, May 2000.
- [16] B Kaimovitz, Y Lanir, and G S Kassab. Large-scale 3-D geometric reconstruction of the porcine coronary arterial vasculature based on detailed anatomical data. *Annals of biomedical engineering*, 33(11):1517–35, November 2005.
- [17] W Schreiner and P F Buxbaum. Computer-optimization of vascular trees. *IEEE transactions on bio-medical engineering*, 40(5):482–91, May 1993.
- [18] B Kaimovitz, Y Lanir, G S Kassab, S Nees, G Juchem, N Eberhorn, M Thallmair, S Förch, M Knott, A Senftl, T Fischlein, B Reichart, D R Weiss, and H G M Van Beek. A full 3-D reconstruction of the entire porcine coronary vasculature. *Am J. Phys. Heart Circ. Phys.*, 299(July 2010):1064–1067, 2010.
- [19] Y Jiang, Z Zhuang, A J Sinusas, and X Papademetris. Vascular Tree Reconstruction by Minimizing A Physiological Functional Cost. *Conference on Computer Vision and Pattern Recognition Workshops IEEE Computer Society Conference on Computer Vision and Pattern Recognition. Workshops*, pages 178–185, June 2010.
- [20] K A McCulloh, J S Sperry, and F R Adler. Water transport in plants obeys Murray’s law. *Nature*, 421(6926):939–942, 2003.
- [21] R Karch, F Neumann, M Neumann, and W Schreiner. Staged growth of optimized arterial model trees. *Annals of biomedical engineering*, 28(5):495–511, May 2000.
- [22] W Schreiner, F Neumann, M Neumann, R Karch, A End, and S M Roedler. Limited Bifurcation Asymmetry in Coronary Arterial Tree Models Generated by Constrained Constructive Optimization. *The Journal of general physiology*, 109(2):129–140, 1997.
- [23] W Schreiner, R Karch, M Neumann, F Neumann, P Szawlowski, and S Roedler. Optimized arterial trees supplying hollow organs. *Medical Engineering & Physics*, 28(5):416–429, 2006.
- [24] M Georg, H Hahn, and T Preusser. Global constructive optimization of vascular systems. *Submitted to IEEE*, (314), 2004.
- [25] S. Kirkpatrick, C. D. Gelatt, and M.P. Vecchi. Optimization by simulated annealing. *Science*, 220:671–680, 1983.

- [26] J. J. J. M. Van Den Broek and M. H. L. M. Van Den Broek. Application of An Ellipsoidal Heart Model In Studying Left Ventricular Contractions. *J. Biomechanics*, 13:493–503, 1980.
- [27] A R Pries and T W Secomb. Origins of heterogeneity in tissue perfusion and metabolism. *Cardiovascular Research*, 81(2):328–335, 2009.
- [28] Y Liu and G S Kassab. Vascular metabolic dissipation in Murray’s law. *American journal of physiology Heart and circulatory physiology*, 292(3):H1336–H1339, 2007.
- [29] H S Frca. Coronary blood flow. *British Journal of Anaesthesia*, 5(2):61–64, 2005.
- [30] S Sunni, S P Bishop, S P Kent, and J C Geer. Diabetic cardiomyopathy. A morphological study of intramyocardial arteries. *Archives of pathology laboratory medicine*, 110(5):375–381, 1986.
- [31] K Johnson, P Sharma, and J Oshinski. Coronary artery flow measurement using navigator echo gated phase contrast magnetic resonance velocity mapping at 3.0 T. *Journal of Biomechanics*, 41(3):595–602, 2008.
- [32] OpenStax College. *Anatomy and Physiology [ISBN 978-1-938168-13-0, Available at Connections Web site, <http://cnx.org/content/col11496/1.6/>]*. June 2013.
- [33] A. M. Gharib, V B Ho, D R Rosing, D A Herzka, M Stuber, A E Arai, and R I Pettigrew. Coronary Artery Anomalies and Variants: Technical Feasibility of Assessment with Coronary MR Angiography at 3 T1. *Radiology*, 247(1):220–227, April 2008.
- [34] B Kaimovitz, Y Huo, Y Lanir, and G S Kassab. Diameter asymmetry of porcine coronary arterial trees: structural and functional implications. *American journal of physiology Heart and circulatory physiology*, 294(2):H714–H723, 2008.
- [35] A Yoldas, E Ozmen, and V Ozdemir. Macroscopic description of the coronary arteries in Swiss albino mice (*Mus musculus*). *Journal of the South African Veterinary Association*, 81(4):247–252, 2010.
- [36] O. Ozgel, A. Haligur, N. Dursun, and E. Karakurum. *Anat. Histol. Embryol*, 33:278–283, 2004.
- [37] Kalyan C Vinnakota and James B Bassingthwaighe. Myocardial density and composition: a basis for calculating intracellular metabolite concentrations. *American journal of physiology. Heart and circulatory physiology*, 286(5):H1742–H1749, 2004.
- [38] N G Uren, J A Melin, B De Bruyne, W Wijns, T Baudhuin, and P G Camici. Relation between myocardial blood flow and the severity of coronary-artery stenosis. *The New England*

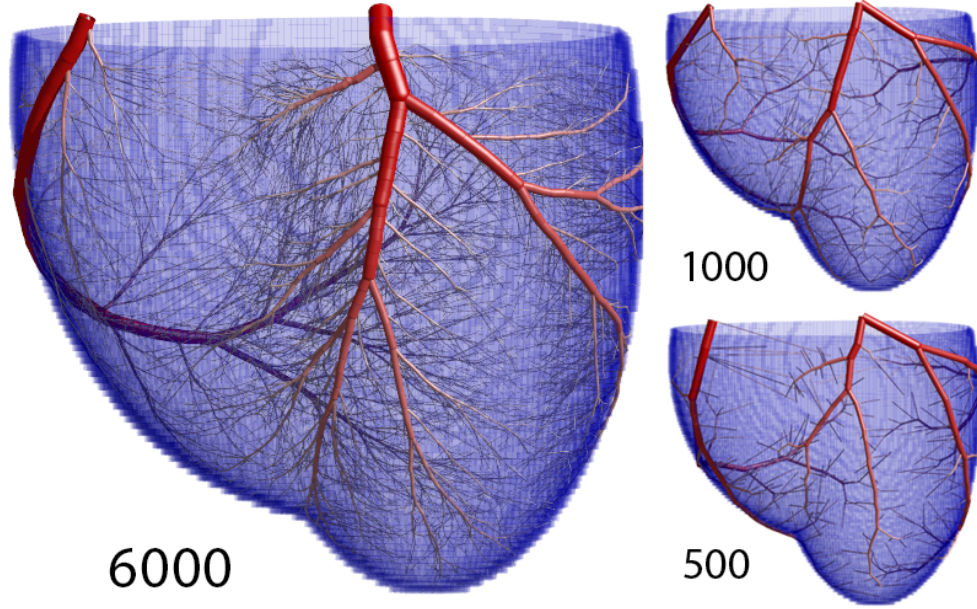


FIG. 1: Images showing arterial trees grown with the algorithm. The number of terminal arterioles is increased from 500 to 6000 (the total number of arterial segments is roughly twice this). There is consistency in the positioning of the larger arteries between the algorithm and the typical arrangement of the major arteries, suggesting that the coronary arteries may be the result of a biological process seeking the global minimum in metabolic demand.

journal of medicine, 330(25):1782–1788, 1994.

- [39] John E Hall. *Guyton and Hall Textbook of Medical Physiology*. 2010.
- [40] J Amanatides and A Woo. A Fast Voxel Traversal Algorithm for Ray Tracing. *Delta*, i(3):3–10, 1987.
- [41] D Henderson, S H Jacobson, and A W Johnson. The theory and practice of simulated annealing. In *Handbook of metaheuristics*, chapter 10, pages 287–319. Kluwer, 2003.
- [42] Z L Jiang, G S Kassab, and Y C Fung. Diameter-defined Strahler system and connectivity matrix of the pulmonary arterial tree. *Journal of Applied Physiology*, 76(2):882–892, 1994.

Acknowledgments EMLC is a British Heart Foundation Intermediate Basic Science Research Fellow (FS/10/46/28350).

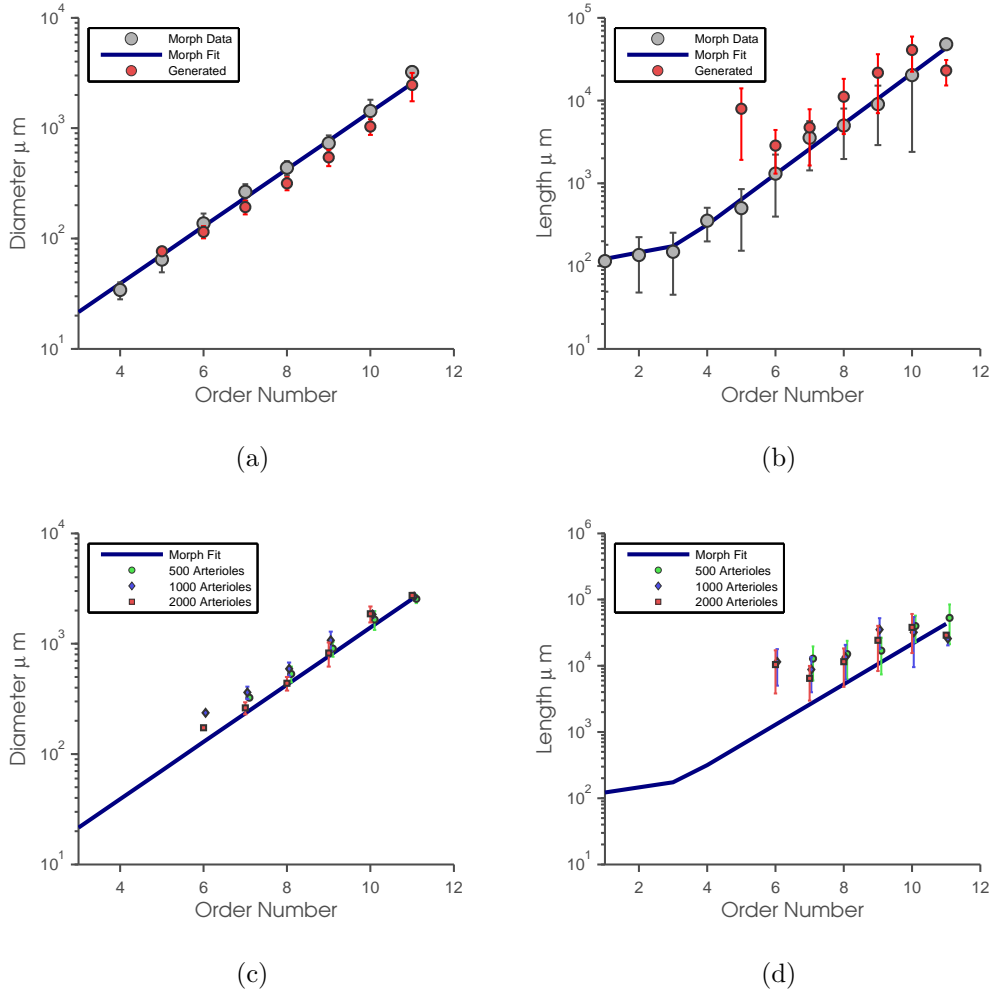


FIG. 2: (a) Vessel diameter as a function of order in a tree with 6000 arterioles. Excellent agreement is found for vessels on all length scales. (b) Vessel length as a function of order number. Agreement is excellent for the major vessels (large order). The large variation seen for arterioles (lower order) is a result of early termination. Also shown are the morphological data reproduced from Table 2 of Ref. [7] for easy comparison. (c) and (d) are as (a) and (b), but for smaller trees to highlight the trend towards the morphological data as tree size increases. (Error bars show standard errors, both axes are logarithmic.)

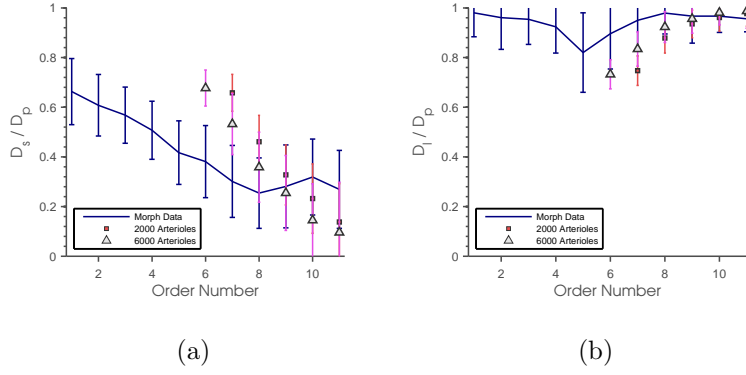


FIG. 3: The ratio of daughter vessel diameters (D_s and D_l are the diameters of the smallest and largest daughter vessels respectively) to diameters of parent segments, D_p as a function of order number, showing how the tree tends towards more symmetric branching at lower orders. Agreement with morphological data reproduced from tables in the online supplement of Ref. [34] is good, if the early termination of the generated trees is taken into account, with the trend towards the morphological data as the tree size increases. Both graphs demonstrate that there are large trunks at high orders with the largest daughter vessel (panel (b)) of similar size to the parent vessel and another side artery which is much smaller (panel (a)). At smaller orders, the ratio becomes similar showing that the branchings of the smaller arteries are near symmetric. Realistic branching asymmetries are a clear advantage over other methods of generating arterial trees *in-silico*.

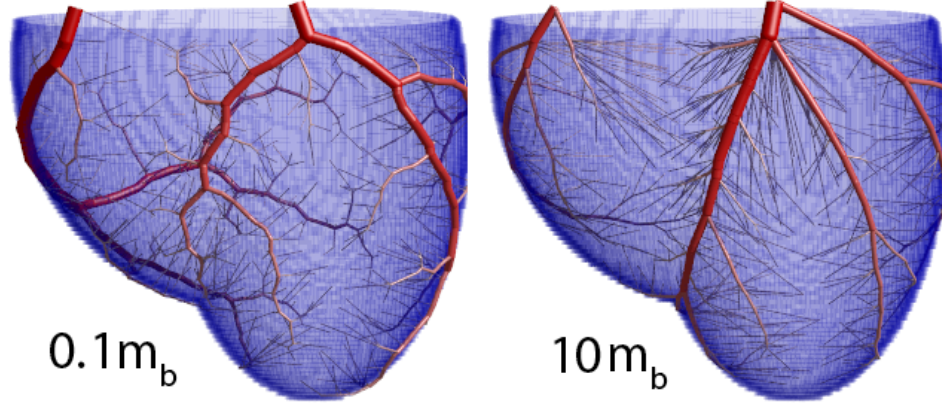


FIG. 4: Example trees generated with different values of m_b , which changes the relative weight of the pumping power to cost of maintaining blood in the optimization. For small m_b (corresponding to small hearts), vessels in the trees wind around - this is because there is little penalty to make a single wide vessel that curves to supply blood, rather than bifurcating. For large m_b (corresponding to large hearts) the vessels travel as straight as possible.

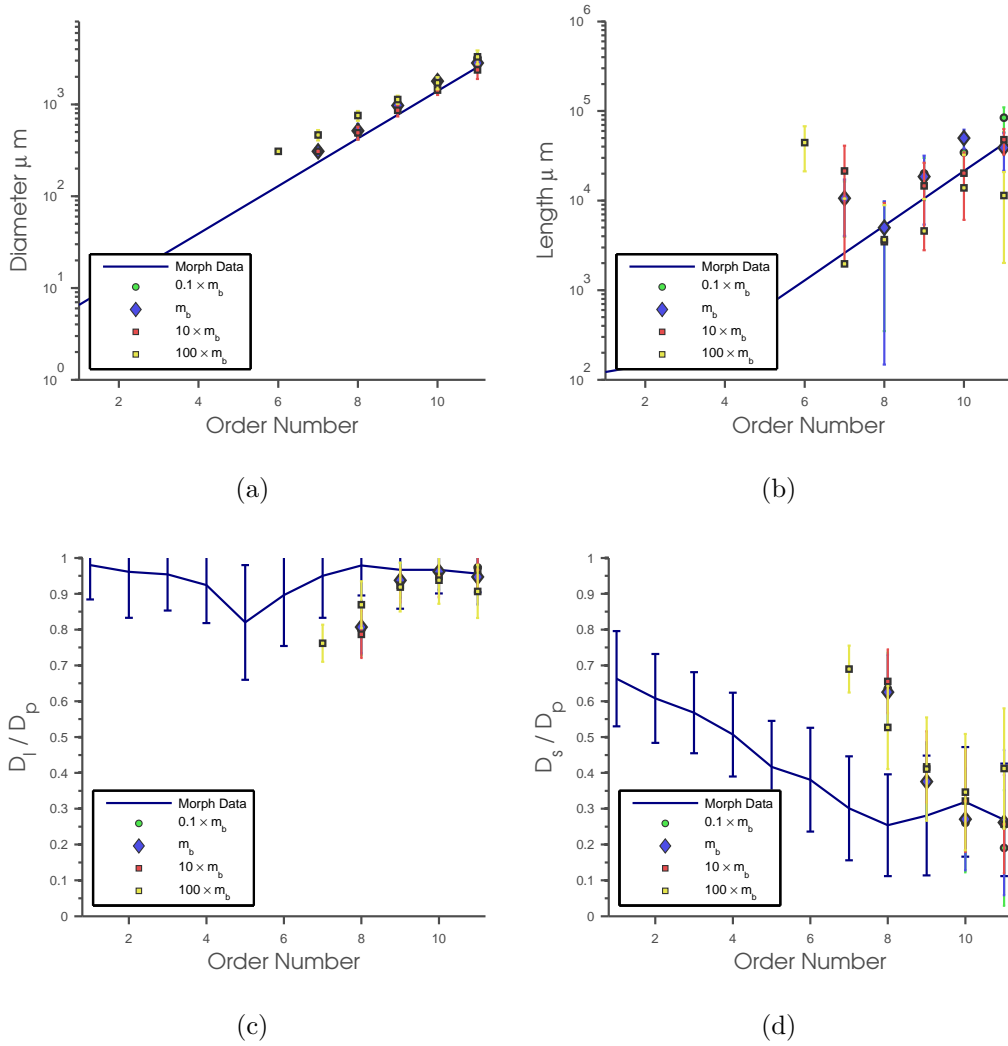


FIG. 5: (a) Diameter as a function of Order Number for trees with 1000 vessels.

Decreasing the volume to power ratio, which describes the relative energy cost of an amount of blood and the power required to pump it, has little effect on the agreement of the diameters with morphological data. (b) For lengths however there is an obvious effect in the larger arteries, with regimes of high pumping cost being more accurate. The primary optimization for high pumping cost then is to increase the length of the largest arteries. (c) and (d) The main effect is a change in the asymmetry of the branching of the largest arteries - for large m_b , the branches are more symmetric than for small m_b . As m_b becomes very small, the limiting behavior is broad trunks that wind around all the tissue, with a large number of very small offshoots that supply blood in the direct vicinity of the large vessel.